Electrochemical preparation and surface properties of gold nanowire arrays formed by the template technique

P. FORRER[1]*, F. SCHLOTTIG[2]*[†], H. SIEGENTHALER[1] and M. TEXTOR[2]

[1]*University of Bern, Department of Chemistry and Biochemistry, Freiestrasse 3, CH-3012 Bern, Switzerland*
[2]*ETH Zürich, Laboratory for Surface Science and Technology, Department of Materials, CH-8092 Zürich, Switzerland*
([†]*Present address: STRATEC Medical, CH-4436 Oberdorf, Switzerland, *authors for correspondence*)

Abstract

A new procedure for preparing free-standing nanowire arrays is described. This is based on a template method which entails electrochemical metal deposition into nanometer-wide parallel pores of porous anodic oxide films on aluminum. By varying the preparation conditions and by applying electrochemical posttreatment methods, gold nanowire arrays are prepared, whose morphological and dimensional properties and oxygen content in the nanowire surface can be varied and investigated by SEM and XPS-characterization. The voltammetric behaviour of such nanowire arrays shows a significant enhancement of the ratio between the total electrolytically exposed surface area and the diffusionally accessible surface area in comparison with macroscopic flat gold electrodes.

1. Introduction

The scientific and technological aspects of nanostructured materials are currently attracting considerable attention. Several procedures have been proposed and applied to the synthesis of nanostructures, such as molecular beam epitaxy and microlithography. A method which entails synthesizing the desired material within the pores of a nanoporous membrane is called 'template synthesis'. The preparation of nanowires of different materials has recently attracted wide attention in view of possible future applications in areas such as photocatalysis, electrochemistry, battery research and enzyme immobilization. There are different concepts of using the pores in nanoporous membranes as templates for preparing nanomaterials [1, 2]. This general template synthesis is an elegant chemical or electrochemical approach for the fabrication of nanostructures, particularly in view of its flexibility to produce nanowires with a different composition. The prepared tubules and fibrils can be composed of conductive polymers [3], semiconductors [4], carbon [5] or other materials.

In this paper free standing nanostructured metal nanowire arrays are prepared by copying exactly a naturally occurring structure. Anodically grown porous alumina, which is known to have a very regular structure, has been chosen as template material, whose structure can be adjusted by variation of the experimental anodization conditions. The morphological and surface properties of the resulting free standing nanowire arrays are investigated by XPS, SEM and TEM, and their electrochemical response is evaluated by cyclic voltammetry and is interpreted in comparison with the electrochemical behaviour of single disc shaped or hemispherical microelectrodes [6–8] and of conventional embedded microelectrode arrays [9–17].

2. Experimental details

2.1. *Electrochemical preparation technique of gold nanowire arrays*

2.1.1. *Anodization*
Nanoporous alumina templates were prepared by anodisation of aluminum. Aluminum sheets (99.9%, 0.5 mm thick, Alusingen, reflector sheets) with a mirror-like surface were cleaned in Almeco 18 (Henkel) and oxidized anodically in phosphoric acid (150 g l^{-1}, 35–70 °C) under the different anodization conditions (voltage, current density and electrolyte temperature in relation to the dimensions of the nanowires) given in Table 1. Two titanium plates were used as counter electrodes.

Figure 1(a) shows schematically a cross section of the porous alumina layer on top of an alumina barrier layer and the aluminum substrate. For the subsequent step of producing metal nucleation sites in the porous layer (Figure 1(b)), it was necessary to decrease the barrier layer thickness at the end of the anodisation process by

Table 1. Influence of the experimental preparation and posttreatment conditions of the nanowire arrays upon length and diameter of the nanowires

Anodization voltage /V	Anodization current density/A cm^{-2}	Anodization time /min	Electrolyte temperature /°C	Approx. length of nanowires/nm	Approx. tip diameter /nm	Tip density /cm^{-2}
52.0	1.2	11.5	50	1300	45	
50.0	1.2	10.5	50	800	40	220×10^8
80.0	1.8	4.0	50	600	38	196×10^8
40.0	1.0	6.0	50	600	38	196×10^8
50.0	1.2	9.5	50	400	33	188×10^8
19.8	12	9.5 s	68.5	100	27	180×10^8
52.0	1.2	11.5 (+ 10 s posttreatment)	50	620	70	422×10^7
52.0	1.2	11.5 (+ 20 s posttreatment)	50	620	80	372×10^7
52.0	1.2	11.5 (+ 30 s posttreatment)	50	570	83	346×10^7

reducing the anodization voltage in small steps, resulting in a modification of both the barrier layer and the pore structure. For such Al_2O_3 films, the pores do not run straight from the top of the membrane to the bottom. Instead, branching on the bottom of the originally straight pores in very small dimensions in the base part is observed [18] (Figure 2).

2.1.2. *Pore filling, wire growth and template removal*
For the deposition of gold into the pores of the alumina film, gold nanoparticles were deposited in the pores by applying an anodic a.c. potential (16 V) in a gold bath (1 g l^{-1} HAuCl$_4$.3H$_2$O + 7 g l^{-1} H$_2$SO$_4$) during 6 s, to provide nucleation sites for the subsequent pore filling step. The nuclei-inoculated pores were filled with a

commercial bath for electroless gold deposition (Auruna® 516, Degussa, Schwäbisch Gmünd, Germany) to produce the nanowires, and in a subsequent step a 15 μm top gold layer was deposited by electroplating using a commercially available gold electroplating bath (Auruna® 552, Degussa). The alumina film and the aluminum base metal were removed in a NaOH solution (50 g l^{-1}, 12 h, 40 °C) to expose a free standing array of nanowires. The resulting array (Figure 1(c)) was first rinsed in water, neutralized in citric acid (50 g l^{-1}), rinsed again in water and in ethanol and then stored in air.

2.2. *SEM, XPS and TEM measurements*

The surface morphology of the nanowire arrays was characterized by scanning electron microscopy (Jeol 840 A), while the surface composition was analysed by X-ray photoelectron spectroscopy (Sage 100 Specs, Berlin) using nonmonochromatized MgK$_\alpha$-radiation and an electron detector pass energy of 50 eV for survey and 14 eV for high resolution scans. Atomic concentrations were calculated from peak area using ionization cross sections published by Scofield [19]. In addition
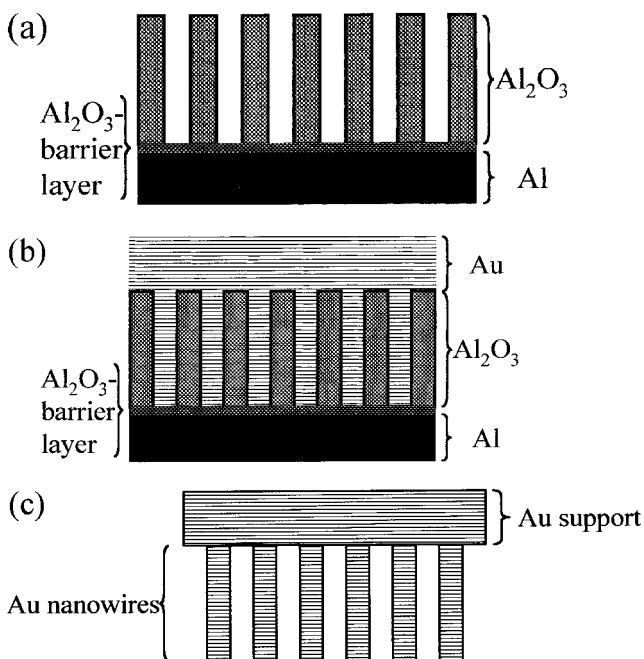

Fig. 1. Schematic view of the preparation procedure of the nanowire array preparation technique. (a) Porous anodic oxide film on aluminum substrate; (b) after metal deposition in and on the oxide film and (c) after selective removal of the aluminum and alumina template.
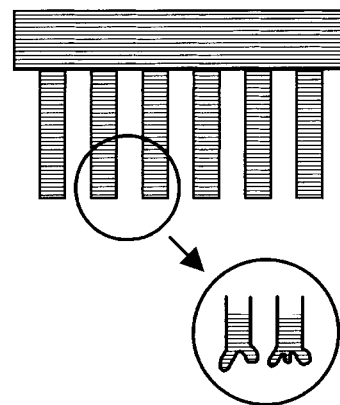

Fig. 2. Schematic view of pore branching at the base of the pores of the anodic oxide film, resulting in branched nanowire tips after pore filling with gold.

transmission electron microscopy (TEM) micrographs of the cross section of the nanowire arrays were recorded using microtome-prepared slices.

2.3. Post-treatment of nanowire array surface

For the electrochemical measurements, a further modification of the morphological properties was necessary, and was done by polishing the nanowire arrays electrochemically using the following procedure [20]: (i) anodic polishing in 1 M H_2SO_4 at a current density of 360 mA cm^{-2} for 20 or 30 s, and (ii) rinsing in MQ-water, 5 M HCl and again MQ-water. For comparative measurements, a mechanically polished flat gold electrode was submitted to the same two-step electrochemical surface polishing procedure.

2.4. Electrochemical measurements and calculations

The electrochemical response of the nanowire arrays was investigated by cyclic voltammetry using the $[Fe(CN)_6]^{4-}/[Fe(CN)_6]^{3-}$-redox couple as a reversible faradaic test system.

All voltammetric measurements were performed in a conventional three-electrode cell using an Autolab potentiostat (Eco-Chemie) with a platinum wire as counter electrode and a saturated mercurous sulfate electrode (MSE, 0.62 V vs. NHE) as reference electrode. The measurements were carried out in 0.5 M Na_2SO_4 with and without $K_4[Fe(CN)_6]$ at different concentrations, prepared from reagent grade chemicals and MQ-water. All potentials are quoted against MSE. Before the measurements, the electrolyte was deaerated for 30 min.

Preliminary test measurements with different scan rates in the range between 0.005 and 0.2 V s^{-1} showed that an intermediate scan rate of 0.1 V s^{-1} provided the differentiation possibility between the capacitive and the faradaic current contributions. This scan rate was then chosen for the systematic measurements. The resulting cyclic voltammograms were processed with the mathematical software Mathcad (Mathsoft). The voltammetric peak currents were evaluated after a base current deduction by an implemented fitting routine.

2.5. Electrode mounting

For the SEM and XPS-measurements the nanowire arrays were used as prepared, or as obtained after the electrochemical posttreatment. For the electrochemical measurements, the nanowire arrays were fixed in a special mounting system (Figure 3). The diameter of the electrochemically exposed electrode area is defined by the dimension of the annular silicon washer (C in Figure 3).

The comparative measurements with the conventional flat gold electrodes were done using the same electrode mounting system.
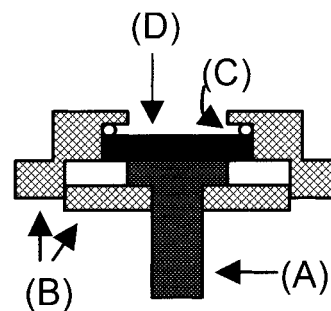

Fig. 3. Special electrode mounting system with brass pin (A), PETP holder (B), silicon washer (C) and nanowire arrays on top of a polycrystalline gold electrode (D).

3. Results and discussion

3.1. Morphological properties and chemical composition

SEM micrographs of free standing nanowire arrays exposed from the alumina template (Figure 4) show that the deposited metal fills the pores uniformly.

The morphological properties of the arrays depend on their preparation conditions (Table 1). Arrays with nanowire lengths in the range of 100 nm to 5 μm could be produced. The average lengths of the nanowires are approximately 800, 600, 400 and 100 nm for the investigated samples.

SEM investigations show that the nanowire lengths are also found to be quite uniform. The accurate determination of the diameters is difficult due to the small lateral distance between the nanowires. Image analysis was used to quantify the nanowire diameters, based on high-resolution SEM micrographs (Quantimet 570, Cambridge Instruments). The morphological properties of the nanowire arrays prepared by different preparation conditions are similar and are dominated by branched features at the upper end of the nanowires, whose diameters are considerably smaller than the diameters of the underlying nanowires.

Figure 5 presents a transmission electron micrograph of a microtomed cross section of a nanowire array, liberated from the template. The electron micrograph suggests a uniform and uninterrupted wire structure for the gold array, where no segmentation or morphological imperfections, such as branching is observed.

The influence of the electrochemical posttreatment upon the dimensional properties of the nanowire arrays is shown in Figure 6 for the example of a 1000 nm wire sample posttreated during 2 different time intervals of 20 and 30 s.

By applying the electrochemical polishing technique, branching of the nanowire tips can be prevented (Figure 6), but the length and diameter of the nanowires changes after applying different treatment times to approximately 600 nm and about 80 nm, respectively.
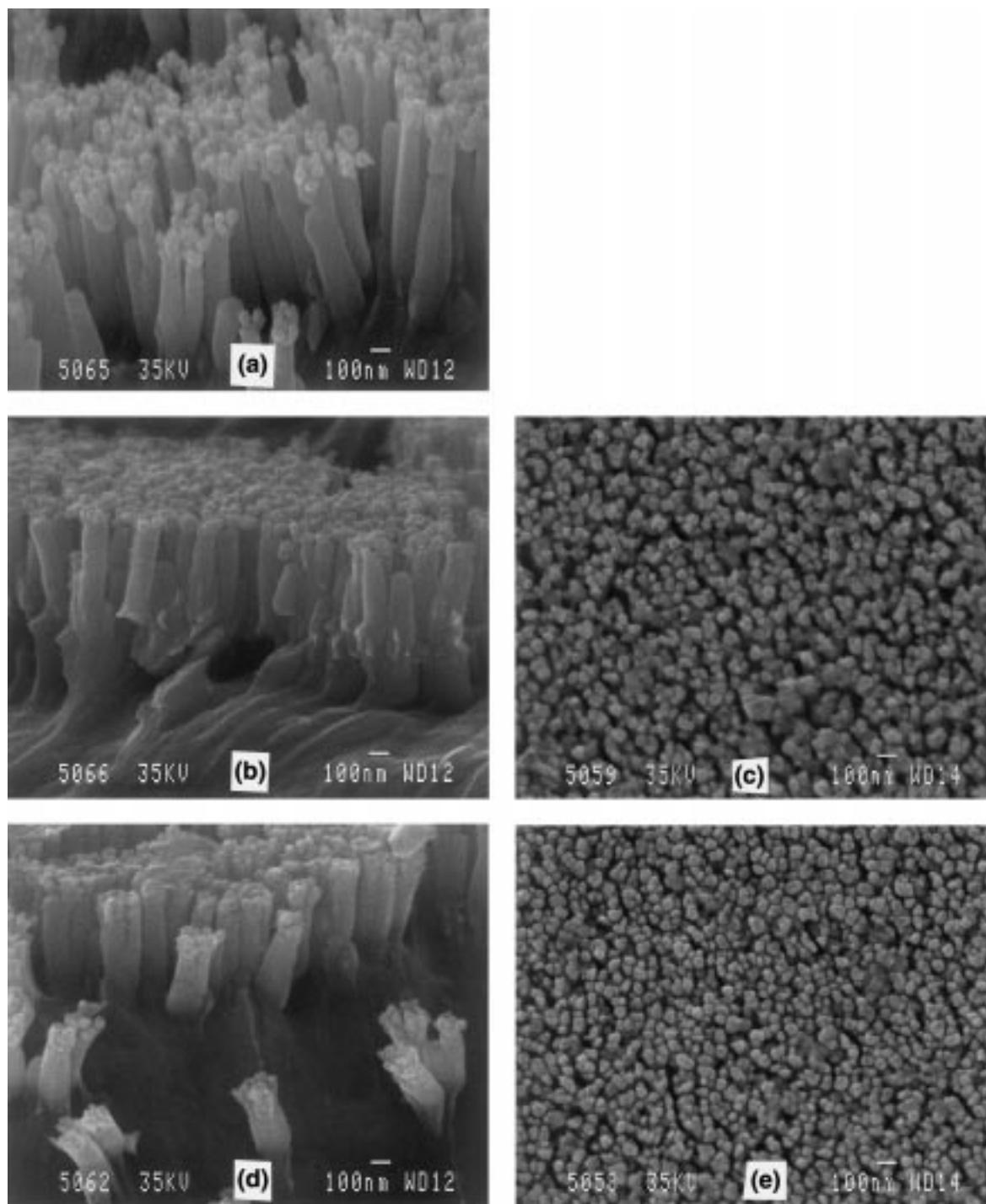
Fig. 4. SEM micrographs of gold nanowire arrays with different nanowire lengths. (a) 800, (b and c) 600 and (d and e) 400 nm.

3.2. *XPS measurements*

The XP spectra of a conventional gold electrode and of the nanowire arrays show characteristic signals corresponding to carbon, oxygen and gold, whereby the oxygen concentration is strongly reduced by the electrochemical post-treatment of the surface (Table 2).

For different surface treatment times, no significant differences in the elemental concentrations were found. The difference between the gold and oxygen content and 100% is mostly due to natural hydrocarbon contamination of the samples. We assume that the higher oxygen content observed before applying the surface treatment process is caused by NaOH passivation during the matrix-removal process [21].

3.3. *Cyclic voltammetry of a reversible redox couple*

3.3.1. *Theoretical considerations*
In the case of diffusion-controlled faradaic reactions at nanowire arrays, the build-up of nonlinear diffusion profiles at the individual nanowires and their time-
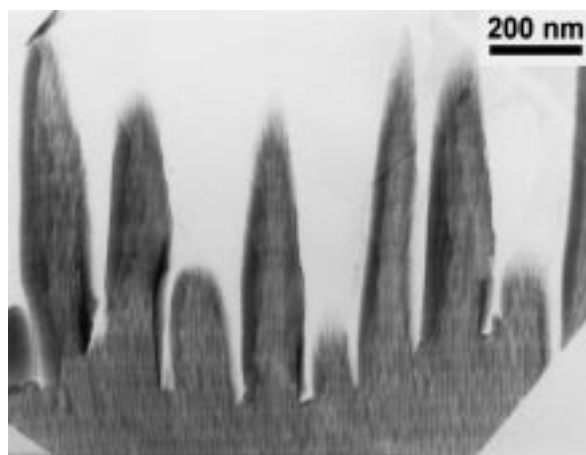
Fig. 5. TEM micrograph of a microtomed cross section of a nanowire array.

Table 2. XPS measurements of the surface oxygen and gold content of nanowire arrays

	Nanowire array, uncleaned	Nanowire array, 20 s surface posttreatment	Nanowire array, 30 s surface posttreatment	Flat gold electrode, 30 s surface posttreatment
Au (at. %)	30.6	30.5	30.0	31.2
O (at. %)	23.4	10.9	11.1	9.5

dependent overlap has to be considered for the assessment of the voltammetric response. This is shown schematically in Figure 7.

Figure 7 (a) shows the diffusional conditions prevailing at the individual nanowires in the case that there is no overlap with the neighboring elements: The diffusional flux at each nanowire is controlled by approximately cylindrical diffusion at the lateral periphery of each nanowire (A), by diffusion at the conducting base substrate between the nanowires (B), and by diffusion (C) at the front surface of each nanowire, which can be considered approximately linear at initial short times and developing into approximately hemispherical diffusion, as encountered at flat disc-shaped microelectrodes.

Under the conditions of this 'individual nonlinear case', the total flux at the nanowire array is given by the sum of all mutually independent fluxes at each nanowire. This case, however, will only prevail, as long as there is no overlap of the laterally expanding cylindrical diffusion layers between the nanowires, i.e. at very short times after the onset of the diffusional flux and at arrays with sufficiently large distances between the nanowires. With increasing time, the diffusion layers around each
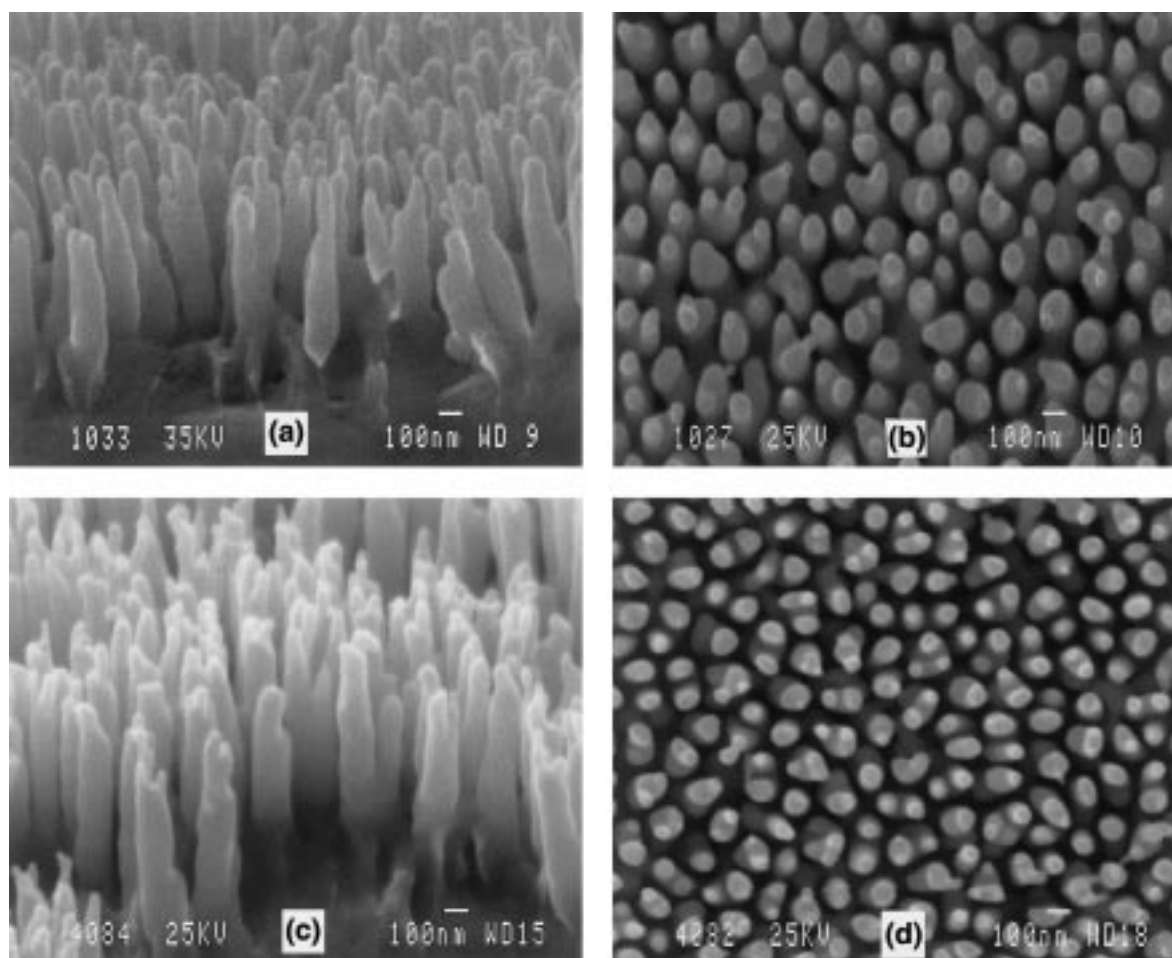

Fig. 6. SEM micrographs of nanowire arrays after electrochemical posttreatment for 20 s (a and b) and 30 s (c and d).
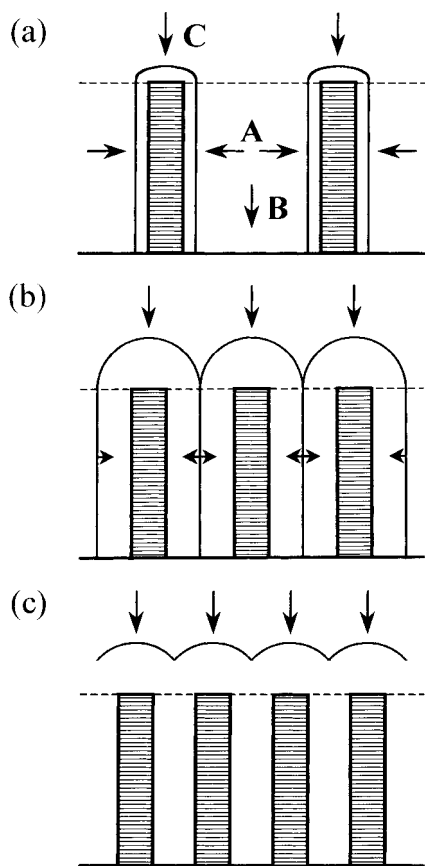
Fig. 7. Schematic presentation of the diffusional conditions prevailing at nanowire array electrodes. (a) Individual nonlinear case; (b) complete overlap case and (c) limiting linear diffusion case.

nanowire expand to complete overlap (Figure 7(b)), and finally a 'limiting linear diffusion case' is reached (Figure 7(c)), where the diffusional flux in the electrolyte

volume elements between the nanowires is completely exhausted, and diffusional transport only occurs between the front surface of the nanowires and the adjoining bulk electrolyte in an approximately linear diffusion pattern.

While the voltammetric response is governed by highly nonlinear diffusion models in the cases of Figure 7(a) and (b), the case of Figure 7(c) is equivalent to linear diffusion at an electrode, whose electrochemically active surface is reduced and given only by the sum of the top surfaces of each nanowire.

3.3.2. *Capacitive behaviour*

Figure 8 shows a comparison of the residual current voltammograms of an electropolished flat gold electrode (a) with a geometric surface area of 0.353 cm^2, and of a posttreated nanowire array electrode (b) with the same geometric surface area, in the supporting electrolyte solution 0.5 M Na$_2$SO$_4$, submitted to electrochemical posttreatment for 30 s.

The nanowire arrays electrode exhibits a much larger residual current with a wide anodic peak at 0.03 V and a broad cathodic double peak at about −0.2 V. Assuming that the residual current is dominated by the capacitive current, and choosing an average capacitive current $|i_c|$ of about 56.3 μA the total electrolytically exposed surface area A_1 of the nanowire arrays can be calculated from an experimentally determined average double layer capacitance $C_d = |i_c|/v$, where v is the potential scan rate (0.1 V s^{-1}). The electrolytically exposed surface area A_1 can then determined from C_d either by considering the specific double layer capacitance of the particular electrode–electrolyte system, or by measuring C_d at an identical electrode with known exposed surface area [10]. In the present experiment, the relationship between
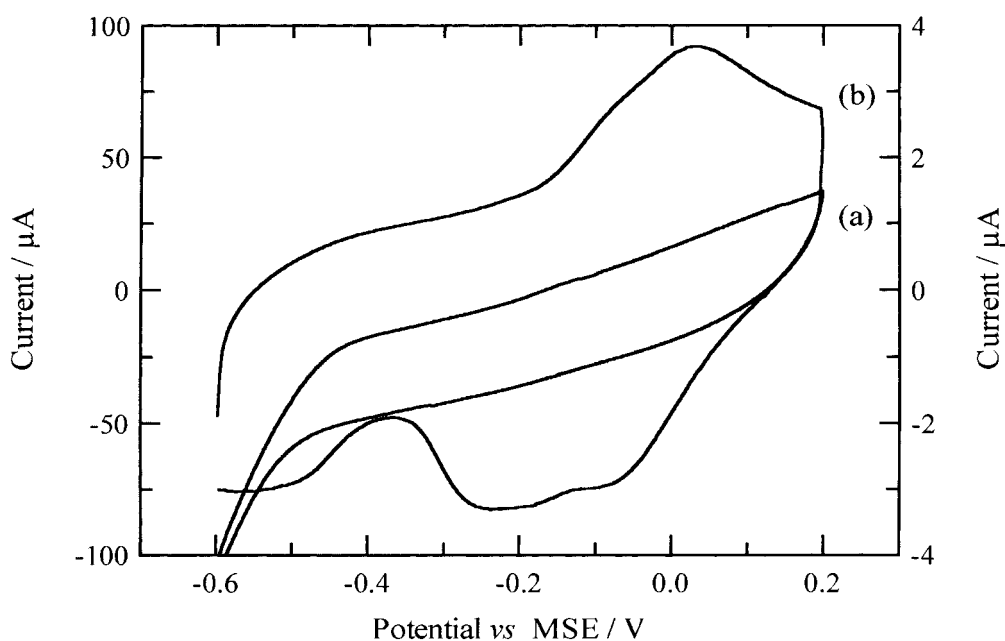
Fig. 8. Cyclic voltammograms recorded in 0.5 M Na$_2$SO$_4$. Scan rate: 0.1 V s^{-1}. (a) Polycrystalline flat gold electrode (right-hand current scale) and (b) nanowire arrays electrode, submitted to posttreatment for 30 s (left-hand current scale).

the measured value of C_d and the exposed surface area has been gained from the flat gold electrode where it can be assumed that the exposed surface area is equal to the geometric area.

Table 3 shows a comparison of the electrolytically exposed surface area A_1 of the flat gold electrode with the electrolytically exposed area A_1 of a nanowire array with identical geometric surface area, and with the sum A_2 of the front areas of all individual nanowires of the array.

The electrolytically exposed area of the nanowire arrays is about 90 times larger than the area of the flat gold electrode and, hence, than its geometric area, whereas the sum of the front area of all individual nanowires amounts to about 50% of the geometric area. A comparison of the two residual current voltammograms in Figure 8 also shows that the anodic and cathodic peaks are only observed at the nanowire arrays. Whether this difference is due to slight differences in the chemical surface composition of the nanowire arrays or due to structural differences, resulting in a change of the potential dependence of the double layer capacitance, remains open.

3.3.3. Voltammetric behaviour of a reversible redox system

Figure 9 shows a comparison of the cyclic voltammograms obtained with the system $[Fe(CN)_6]^{4-/3-}$ in 0.5 M Na_2SO_4 at nanowire arrays with various nanowire lengths (a–d) without posttreatment, and at a flat gold electrode (e) with identical geometric surface area. An additional comparison between a flat gold electrode and a posttreated nanowire array is shown in Figure 10. The voltammograms recorded at the nanowire arrays differ from the voltammogram recorded at the flat gold electrode by the higher capacitive currents, that increase

Table 3. Quantities determined from cyclic voltammograms for total surface area exposed to the electrolyte (A_1) and sum of the front areas of all nanowires of a nanowire array exposed to the electrolyte (A_2)

Electrode	A_1/cm^2	A_2/cm^2
Polycrystalline flat gold electrode	0.353	
Nanowire arrays posttreated for 30 s	31.8	0.185

with increasing length of the nanowires and, hence, increasing electrolytically exposed surface area.

The faradaic redox transfer of the Fe^{II+}/Fe^{III+} system results in a pronounced cathodic and anodic wave, whose potentials coincide with the peak potentials of the voltammogram recorded at the flat gold electrode. The heights of theses faradaic redox peaks at the nanowire arrays are noticeably lower than the redox peaks recorded at the flat gold electrode. This is more clearly visible in the voltammograms of Figure 10, where the faradaic peak heights at the nanowire array are about half of the peak height at the flat gold electrode, in close similarity to the ratio between the sum A_2 of the front areas of all nanowires (Table 3) and the geometric area of the nanowire arrays, that equals the area A_1 of the flat gold electrode in Table 3.

The voltammograms recorded at the nanowire arrays without posttreatment (Figure 9(a) to (d)) and with posttreatment (Figure 10(b)) show no significant differences in the voltammetric peaks of the faradaic reaction, but differ at the anodic potential limit by the occurrence of an additional cathodic and anodic peak at the posttreated array, as recorded also in the corresponding
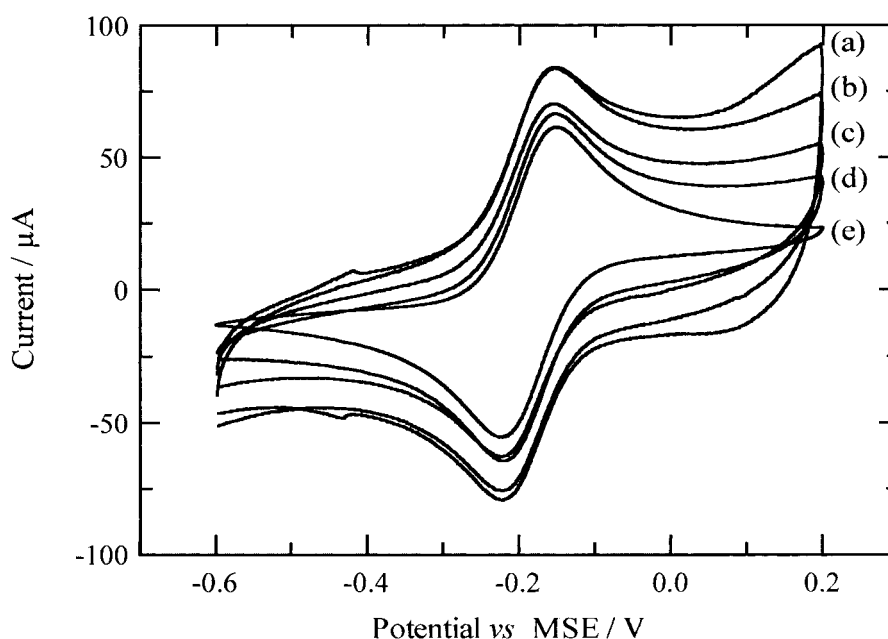

Fig. 9. Cyclic voltammograms in 0.5 M Na_2SO_4 + 10^{-3} M $K_4[Fe(CN)_6]$ of nanowire arrays electrodes with different lengths: (a) 800, (b) 600 (c) 400, (d) 100 nm and (e) Flat gold electrode. Scan rate: 0.1 V s^{-1}.
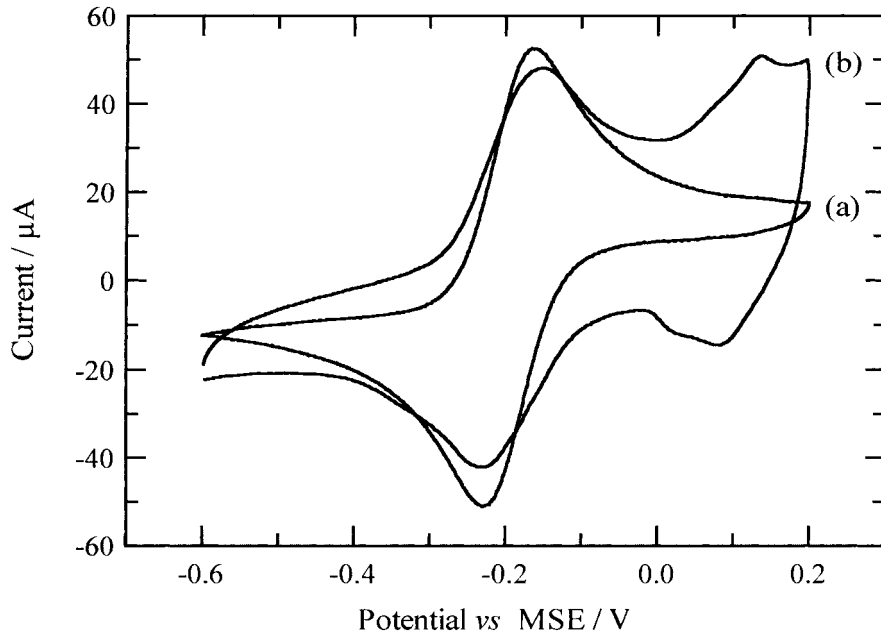
Fig. 10. Cyclic voltammograms in 0.5 M Na_2SO_4 + 10^{-3} M $K_4[Fe(CN)_6]$ of nanowire arrays electrodes with different length. (a) Flat gold electrode and (b) posttreated nanowire arrays electrode. Scan rate: 0.1 V s^{-1}.

residual current voltammogram. As already pointed out in the previous part, it is not clear if this difference results from post-treatment-induced changes in the surface structure of the nanowires, or from a contamination effect.

Figure 11 shows double-logarithmic plots of the dependence of the corrected cathodic peak currents on the potential scan rate for a flat gold electrode and a posttreated nanowire array at two different concentrations of $[Fe(CN)_6]^{4-}$ together with a slope of 0.5
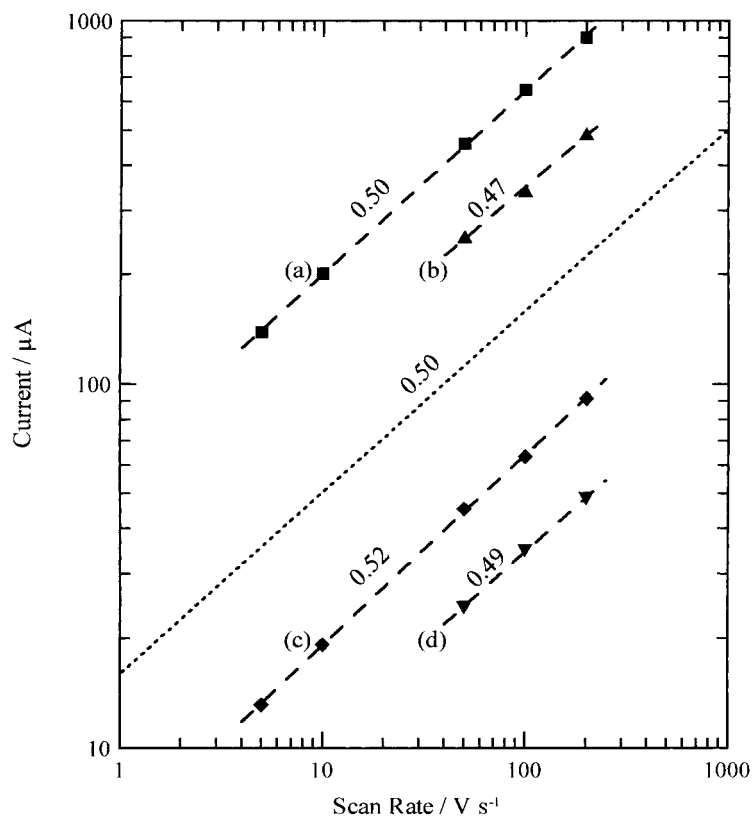

Fig. 11. Log i against log v plot of cathodic peak current. Flat gold electrode in (a) 0.5 M Na_2SO_4 + 10^{-2} M $K_4[Fe(CN)_6]$ and (c) 0.5 M Na_2SO_4 + 10^{-3} M $K_4[Fe(CN)_6]$; posttreated nanowire arrays electrode in (b) 0.5 M Na_2SO_4 + 10^{-2} M $K_4[Fe(CN)_6]$ and (d) 0.5 M Na_2SO_4 + 10^{-3} M $K_4[Fe(CN)_6]$.

corresponding to the proportionality $i \propto 0.5\,v$ that is expected for a redox process controlled by linear diffusion.

Although the plots obtained with the flat gold electrode exhibit slopes of 0.50 and 0.52, the slopes recorded at the nanowire array are slightly lower with values of 0.47 and 0.49. In view of the limited number of data points and of the uncertainties related with the residual current correction, this difference is not considered significant, and good agreement with the behaviour of a system controlled by linear diffusion is thus obtained.

The observed results at the nanowire arrays are consistent with a faradaic reaction controlled by linear diffusion at an electrode with a reduced electrochemically active surface area, corresponding approximately to the sum A_2 of the front surface areas of all nanowires. This can be explained by the assumption that under the applied polarization conditions the limiting linear diffusion case (Figure 7(c)) holds for the flux profile at the nanowire arrays. Under these conditions the electrolyte volume elements between the nanowires are almost immediately fully exhausted, and the only diffusional flux remains on top of the front area of each nanowire.

The time scale for the transition from the individual nonlinear case (Figure 7(a)) to the limiting linear diffusion case (Figure 7(c)) can be estimated from the time interval required for the complete diffusional exhaustion of the electroactive species in the electrolyte element between two nanowires.

Assuming an average lateral distance of less than 200 nm between two nanowires, this amounts to very short time intervals in the order of magnitude of about 10 μs. It is therefore clear, that only the limiting linear diffusion case (Figure 7(c)) applies under the experimental conditions of the faradaic reaction.

4. Conclusion

The newly described template procedure enables the preparation of nanowire arrays with the attractive possibility to vary the height and diameter of the nanowires by the specific preparation conditions. SEM experiments show that an electrochemical posttreatment procedure removes morphological irregularities at the nanowire tips and decreases the oxygen content at the surface.

The voltammetric behaviour of the nanowire arrays is characterized by high capacitive currents due to the large electrode area in contact with the electrolyte, whereas the flux of faradaic processes is restricted to the relatively small surface area given by the sum of the front areas of all nanowires. This results in an electrode system, where the ratio between faradaic and capacitive current signals is markedly reduced in comparison with macroscopic flat electrodes. Such electrodes may therefore serve as electrolytic sensor systems that require a large internal surface, combined with low sensitivity to unwanted faradaic processes.

References

1. C.R. Martin, *Science* **266** (1994) 1961.
2. D. Routkevitch, A.A. Tager, J. Haruyama, D. Almawlawi, M. Moskovits and J.M. Xu, *IEEE Trans. Electron Devices* **43** (1996) 1646.
3. R. Parthasarathy and C.R. Martin, *Nature* **369** (1994) 298.
4. D. Routkevitch, T. Bigioni, M, Moskovits and J.M. Xu, *J. Phys. Chem.* **100** (1996) 14037.
5. T. Kyotani, L. Tsai and A. Tomita, *Chem. Mater.* **8** (1996) 2109.
6. M.F. Bento, M.J. Medeiros, M.I. Montenegro, C. Beriot and D. Pletcher, *J. Electroanal. Chem.* **345** (1993) 273.
7. Z.J. Karpinski and R.A. Osteryoung, *J. Electroanal. Chem.* **349** (1993) 285.
8. C.P. Smith and H.S. White, *Anal. Chem.* **65** (1993) 3343.
9. B.R. Scharifker, *J. Electroanal. Chem.* **240** (1988) 61.
10. V.P. Menon and C.R. Martin, *Anal. Chem.* **67** (1995) 1920.
11. C. Amatore, J.M. Savéant and D. Tessier, *J. Electroanal. Chem.* **147** (1983) 39.
12. F.N. Büchi, PhD thesis, Universität Bern (1989).
13. T. Gueshi, K. Tokuda and H. Matsuda, *J. Electroanal. Chem.* **89** (1978) 247.
14. T. Gueshi, K. Tokuda and H. Matsuda, *J. Electroanal. Chem.* **101** (1979) 29.
15. T. Gueshi, K. Tokuda and H. Matsuda, *J. Electroanal. Chem.* **102** (1979) 41.
16. I.F. Cheng and C.R. Martin, *Anal. Chem.* **60** (1988) 2163.
17. J.C. Hulteen, V.P. Menon and C.R. Martin, *J. Chem. Soc., Faraday Trans.* **92** (1996) 4029.
18. R.C. Furneaux, W.R. Rigby and A.P. Davidson, *Nature* **337** (1989) 147.
19. J.H. Scofield, *J. Electron Spectrosc.* **8** (1976) 129.
20. M. Binggeli, Diploma thesis, Universität Bern (1990).
21. F. Schlottig, M. Textor, N.D. Spencer, K. Sekinger, U. Schnaut and J.-F. Paulet, *Fresenius J. Anal. Chem.* **361** (1998) 684.